A mechanical model of retinal detachment

2012 Phys. Biol. 9 046001

(http://iopscience.iop.org/1478-3975/9/4/046001)

Phys. Biol. **9** (2012) 046001 (9pp) doi:10.1088/1478-3975/9/4/046001

A mechanical model of retinal detachment

Tom Chou[1] **and Michael Siegel**[2]

[1] Departments of Biomathematics and Mathematics, UCLA, Los Angeles, CA 90095-1766, USA
[2] Department of Mathematical Sciences and Center for Applied Mathematics and Statistics, New Jersey Institute of Technology, Newark, NJ 07102-1982, USA

E-mail: tomchou@ucla.edu

Received 24 March 2012
Accepted for publication 21 May 2012
Published 25 June 2012
Online at stacks.iop.org/PhysBio/9/046001

Abstract
We present a model of the mechanical and fluid forces associated with exudative retinal detachments where the retinal photoreceptor cells separate, typically from the underlying retinal pigment epithelium (RPE). By computing the total fluid volume flow arising from transretinal, vascular and RPE pump currents, we determine the conditions under which the subretinal fluid pressure exceeds the maximum yield stress holding the retina and RPE together, giving rise to an irreversible, extended retinal delamination. We also investigate localized, blister-like retinal detachments by balancing mechanical tension in the retina with both the retina–RPE adhesion energy and the hydraulic pressure jump across the retina. For detachments induced by traction forces, we find a critical radius beyond which the blister is unstable to growth. Growth of a detached blister can also be driven by inflamed lesions in which the tissue has a higher choroidal hydraulic conductivity, has insufficient RPE pump activity, or has defective adhesion bonds. We determine the parameter regimes in which the blister either becomes unstable to growth, remains stable and finite-sized, or shrinks, allowing possible healing. The corresponding stable blister radius and shape are calculated. Our analysis provides a quantitative description of the physical mechanisms involved in exudative retinal detachments and can help guide the development of retinal reattachment protocols or preventative procedures.

(Some figures may appear in colour only in the online journal)

1. Introduction

The retina is composed of multiple layers of photoreceptor and nerve cells that sit atop the retinal pigment epithelium (RPE). The RPE is a monolayer of cells attached to Bruch's membrane, a 2–4 μm elastic collagen layer that covers the choriocapillaris, the inner, vascular part of the choroid substrate. The choriocapillaris is the part of the choroid that feeds the metabolically active RPE and retina. Separations between cell layers give rise to retinal detachments that are a major contributor to retinal tissue death and permanent vision loss [1]. The two common types of detachments are rhegmatogenous, in which a hole or tear forms in the thin retinal layer that has separated from the choroid, and exudative, in which a blister forms without a retinal hole (shown in figure 1) [2]. The latter type of detachment is typically associated with vitreous forces that pull the retina from the RPE, or with inflammation or vascular abnormalities that result in pockets of accumulated subretinal fluid, without tearing the retina. In figure 1(*a*), a large blister has formed between the retina and the RPE layer. While this is the typical location of blister formation, separation of the RPE cell layer (red curves) from Bruch's membrane that covers the choriocapillaris can also occur, as shown by the small blister in figures 1(*a*) and (*b*).

There exist numerous clinical protocols for preventing and treating detached retinas, including vitrectomy, laser photocoagulation, scleral buckling [3] and pneumatic retinopexy [1, 2]. These methods exploit different mechanical forces and are used in different circumstances. For example, vitrectomies sever the attachment of the vitreous humor to the detached retina, laser photocoagulation induces injury, allowing a stronger re-adhesion of the scar tissue, and pneumatic retinopexy (injection of a gas bubble to envelope a torn retinal flap) [4].

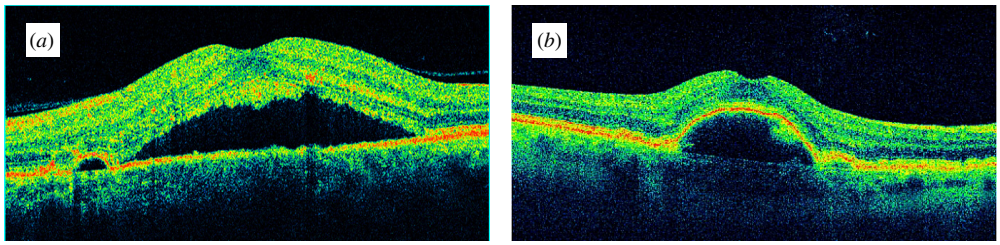

Figure 1. Optical coherence tomography image of exudative retinal detachments. The transverse dimension of each image is approximately 3 mm. (*a*) Exudative retinal detachment in which the retinal photoreceptor layer has separated from the RPE cell layer. The small blister on the left has lifted the RPE from the choroid as in (*b*). (*b*) Detachment in which the RPE layer (red) has separated from the choroid substrate. Used with permission from Dr T Bennett, CRA, FOPS and the Ophthalmic Photographers' Society.

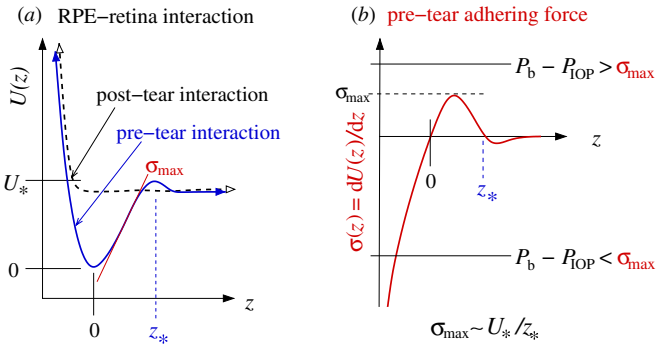

Figure 2. (*a*) The intrinsic adhesion energy per area $U(z)$ between retinal layer cells and the RPE, uniformly separated by distance z. The interaction is defined at a reference pressure difference where $P_b = P_{IOP}$ (see figure 3). At this reference pressure difference, the RPE–retina binding energy per area is defined by U_*. The pre-tear interaction is shown by the solid blue curve. When the displacement extends beyond z_*, bonds are irreversibly broken, and the attractive interaction potential is destroyed (black dashed curve). (*b*) The *adhesive* force per area (stress) $\sigma(z)$ between the two cell layers. The maximum yield stress $\sigma_{max} \sim U_*/z_*$ is also indicated.

Despite the physical forces implicated in retinal detachment and many existing protocols for reattachment [5], a quantitative description of the underlying mechanics is lacking. In this paper, we develop a mathematical model of exudative retinal detachments which incorporates the relevant fluid flows, mechanical tensions and cellular adhesion forces.

2. Retinal structure, forces and flows

The basic forces associated with retinal detachment include pressure-driven flows, active RPE pump flows, cell–cell adhesion forces and possibly retinal tension forces. Retinal photoreceptor cells normally adhere to the RPE. A schematic of a typical macromolecular adhesion interaction between adjacent cells is shown in figure 2. In the absence of hydraulic forces, the cellular adhesion potential $U(z)$ exhibits a minimum at $z = 0$, corresponding to the equilibrium adhesion bond length between apposed retinal and RPE cells. The *adhesive* force per area (stress) between the two cell layers is defined as

$$\sigma(z) \equiv \frac{dU(z)}{dz} \quad \text{for} \quad z < z^*, \tag{1}$$

where $z < z^*$ corresponds to the maximum separation that can be sustained by the tissue. The corresponding stress maximum yield stress that can be sustained is approximately $\sigma_{max} \sim U_*/z_*$.

In addition to cellular adhesion, forces arise from pressure-driven fluid flows across the different tissue layers. Assuming that the fluid pressure in the choriocapillaris is P_c and the intraocular pressure of the vitreous humor is P_{IOP}, the total pressure difference across the entire system is $P_c - P_{IOP}$. Both P_c and P_{IOP} are measurable and somewhat controllable. The capillary pressure is related to the venous blood pressure, while the intraocular pressure P_{IOP} is controlled by the total flow of vitreous humor, which is produced by the ciliary body at the base of the iris and drains predominantly through the trabecular meshwork at the perimeter of the cornea [6–8]. Since $\Delta P \equiv P_c - P_{IOP} \simeq 5$–$10$ mm Hg [9], the higher vascular pressure drives fluid flow from the choriocapillaris to the inner eye in the absence of other active processes.

We also define a fluid pressure P_b in the narrow extracellular space between the RPE and retina that contains the adhesion bonds (see figure 3). Given any specific state of the eye, we will assume that P_{IOP} and P_c are known parameters that can be determined from measurements (e.g., tonometry and blood pressure), but that the subretinal pressure P_b is determined by fluid flow through the choroid and retinal layer. When external separation forces exceed U_*, the cellular adhesion bonds rupture irreversibly. Differences between P_b and P_{IOP} will tilt the potential $U(z) \to U(z) - z(P_b - P_{IOP})$, changing the effective detachment energy per area to $U_* - z_*(P_b - P_{IOP})$.

Pressure-driven fluid flows cross between the choroid space and the subretinal space, and between the subretinal space and the vitreous space. The corresponding volume fluxes, J_c and J_r, are expressed as

$$J_c = L_c(P_c - P_b), \quad \text{and} \quad J_r = L_r(P_b - P_{IOP}), \tag{2}$$

where L_c and L_r are the effective hydraulic conductivities of the choriocapillaris (including that of the RPE and Bruch's membrane) and the retina, respectively. These conductivities will depend on the physiological state of the tissue. For example, loss of integrity of the tight junctions between the RPE cells or inflammation of the choriocapillaris may increase substrate leakiness and L_c. The permeability of Bruch's membrane has also been shown to increase with age [10], decreasing L_c. Nonetheless, if $P_c > P_{IOP}$, passive flows alone will tend to separate the retina from the substrate.

In addition to passive flows, there is a component of the volume flux that is actively pumped by the RPE layer.

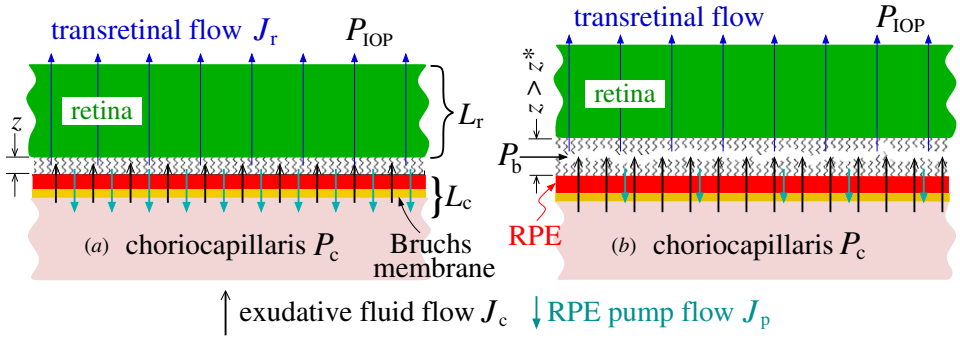

Figure 3. Schematic of a uniform exudative retinal detachment. The retina, RPE, Bruch's membrane and choriocapillaris are colored green, red, gold and pink, respectively. The tissue hydraulic conductivities, intraocular and choroidal pressures, P_{IOP} and P_c, and expected flow directions are labeled. In (*a*), the RPE pumps are active and the indicated passive fluid flow direction results from $P_c > P_b > P_{IOP}$. In this case, the retinal is stable against delamination at the retina–RPE interface. (*b*) If P_c is increased, and/or the RPE pump flux J_p is decreased, fluid accumulates at the retina–RPE interface, irreversibly separating the cell layers. The resulting delamination can only be reattached by changing conditions to those that allow drainage of the interstitial fluid.

The RPE cell layer is special in that it actively pumps fluid from the retinal space through Bruch's membrane and back into the choroid [2]. This volume flux derives from active cellular processes and thus depends on the physiological state of the RPE, and possibly on the trans-RPE hydrostatic pressure difference $P_b - P_c > 0$. However, since RPE pumps are highly metabolic and regulated, we will assume that J_p is independent of $P_b - P_c$ for physiologically representative pressures [11]. Since active RPE pumping is thought to provide an important force keeping the retina attached to the choroid [12, 13], the position and physiological state of the RPE cell layer is an important component of our model. In our analysis, we assume J_p is a pressure-independent parameter that depends on the state of the RPE cells and the regulation mechanisms affecting the pumps.

Table A1 in the appendix lists the parameters used in our modeling and discusses their ranges of values. Whenever possible, our results will be evaluated and discussed within a reasonable range of experimentally measured parameter values.

3. Uniform retinal detachments

First, we consider the stability of attached retina against large, uniform delamination from the RPE. In the presence of fluid flow, static equilibrium requires that the volume flow into the subretinal space balances the flow out of it:

$$J_c = J_r + J_p. \tag{3}$$

Upon using equations (2) in equation (3), we solve for the hydrodynamic pressure difference $P_b - P_{IOP}$ tending to separate the retina from the RPE, and balance this stress with the membrane adhesion force $\sigma(z)$ from equation (1):

$$P_b - P_{IOP} = \frac{L_c \Delta P}{L_r + L_c} - \frac{J_p}{L_r + L_c} = \sigma(z), \tag{4}$$

where $\Delta P \equiv P_c - P_{IOP}$. For a given stress function $\sigma(z) \equiv dU(z)/dz$, equation (4) can be solved to find the cellular layer separation z as a function of ΔP, the RPE pumping flux J_p, and the tissue permeabilities L_r, L_c.

When $\Delta P < 0$, equation (4) can be satisfied only if $\sigma(z)$ is negative. In this regime, the outward passive flow compresses the retina onto the choroid and detachments can occur only through external traction forces from the vitreous humor. On the other hand, when $\Delta P > 0$ is sufficiently large, and/or the RPE pump flux J_p is sufficiently small, the fluid pressure could push the layers to a new equilibrium separation $z > 0$. In cases where $P_b - P_{IOP} > \max\{dU(z)/dz\} \equiv \sigma_{max}$, the maximum yield stress is exceeded; there is no value of z that can satisfy equation (4), and the retina irreversibly rips from the RPE (figure 2(*b*)). Thus, when

$$\frac{L_c \Delta P}{L_r + L_c} - \frac{J_p}{L_r + L_c} > \sigma_{max}, \tag{5}$$

an exudative retinal detachment of infinite extent spontaneously forms. Figure 3(*b*) shows the flows and pressures at which the retina and RPE have irreversibly separated. Condition (5) is one of our main results and shows that if $L_c(P_c - P_{IOP})/(L_r + L_c) < \sigma_{max}$, an exudative detachment cannot arise solely from RPE pump failure ($J_p \to 0$).

Using experimentally determined parameter values listed in table A1, we find that for a reasonable effective bond length $z_* \sim 10^{-7}$m, a loss of RPE pump function will typically not give rise to spontaneous uniform delamination unless $U_* \lesssim 10^{-4}$ J m^{-2}, which is much smaller than typically measured values [14]. Therefore, loss of RPE function alone is insufficient to induce large-scale delamination, which requires external traction forces. However, we will show that loss of RPE pump function can dramatically affect the size and stability of a localized pre-existing retinal blister.

4. Retinal blisters

We now consider retinal blisters that result from local traction forces from the vitreous, or from local heterogeneities in the physiological state of the tissue. The basic geometry of a localized retinal blister is approximated by a spherical cap with radius of curvature R as depicted in figure 4. The circular footprint of the blister is denoted $A_d \equiv \pi R_\perp^2$, while the cap area of the detached retina is A_r. A lesion of inflamed tissue, if it exists, will have area $A_\ell \leqslant A_d$. The tissue within this lesion

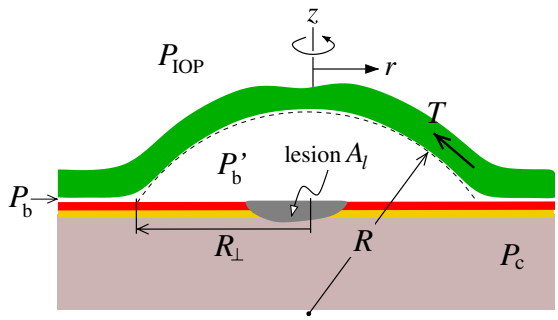

Figure 4. Schematic of a retinal blister. The intraocular pressure, the pressure in the blister and the effective pressure underneath the attached retina are denoted as P_{IOP}, P_b' and P_b, respectively. The blister geometry is defined by a spherical cap with radius of curvature R and footprint radius $R_\perp$. A localized lesion with area A_l may exist within the blister.

may be inflamed with diminished RPE pump activity $\tilde{J}_p'$ or increased tissue permeability.

We assume that there is negligible lateral fluid flow between the blister interior and the infinitesimally thin extracellular space between the retina and the RPE, and that the two pressures P_b' and P_b are independently approximated by the fluid flow through each of the spaces, respectively [15]. Moreover, we neglect the tamponading forces that might arise from the gel-like vitreous inside the eye. This assumption is appropriate for older patients where the vitreous humor has liquefied, and for patients who have undergone vitrectomy. For a blister with the geometry shown in figure 4, static equilibrium is achieved only when the appropriate pressure and retinal tension forces are balanced and there is no net volume flow into the blister. Our problem superficially resembles one-dimensional, classic, static problems in elastica as reviewed by Wang [16] and subsequently extended to include inertial dynamics [17–19]. However, in our retinal detachment problem, we must consider a two-dimensional detached blister, the cellular adhesion energy between retina and substrate, and the evacuating fluid flow generated by the RPE.

According to Laplace's law, the pressure difference $P_b' - P_{IOP}$ must be balanced by the retinal tension T times its curvature:

$$P_b' - P_{IOP} = \frac{2T}{R}. \tag{6}$$

Stability at the contact perimeter of the blister requires balancing of the tension T and the binding energy per unit area $U(z)$ holding the retina to the RPE in the undetached region. If the cellular bonds are ruptured by the total magnitude of the tension force, the tension in the detached retina will obey

$$T \lesssim U_* - z_*(P_b - P_{IOP}) \approx U_*. \tag{7}$$

Equation (7) represents the external stress required to pull off unit area of retina that is attached to the RPE in the presence of the pressures P_b and P_{IOP}. Henceforth, we assume that the region outside the localized blister is far from being delaminated by fluid flow and that $P_b - P_{IOP} \ll \sigma_{max} \approx U_*/z_*$. Therefore, we can safely accept the last approximation $U_* - z_*(P_b - P_{IOP}) \approx U_*$. In the appendix, we describe a more general rupturing relation that takes into account the angle at which the tension is applied.

With suitable constitutive relations between the pressure P_b' and the tension T and the blister geometry, equations (6) and (7) can be used to determine stable blister geometries and sizes. In contrast to, say, a liquid–gas interface, the tension T in our problem is not constant but depends on the amount of stretching the detached membrane suffers, relative to the flat, undetached retina. If we assume that the detached retina resists stretching with a force linearly proportional to the amount of excess area, the tension T will depend explicitly on the dimensionless shape ratio

$$f \equiv \frac{A_d}{A_r} = \frac{\pi R_\perp^2}{A_r}, \tag{8}$$

according to

$$T(f) = Ed\frac{(A_r - A_d)}{A_d} = Ed\left(\frac{1}{f} - 1\right), \tag{9}$$

where E is Young's modulus of the detached retina and d is its thickness. The combination Ed represents the stretching elasticity of the detached retina. Geometrically, the radius of curvature R can be expressed as

$$R(f) = \frac{A_r}{\sqrt{4\pi(A_r - A_d)}} = \frac{R_\perp}{2\sqrt{f(1-f)}}. \tag{10}$$

Finally, it will prove convenient to nondimensionalize all hydraulic conductivities by L_c, all pressures by ΔP, all fluxes by $L_c\Delta P$, and the tension and adhesion energy by Ed. Our new dimensionless variables are defined by

$$\tilde{J}_p = \frac{J_p}{L_c\Delta P}, \quad \tilde{L}_r = \frac{L_r}{L_c}, \quad \text{and} \quad \tilde{U}_* = \frac{U_*}{Ed}. \tag{11}$$

Upon using expressions (9) and (10) for $T(f)$ and $R(f)$ in equations (6) and (7), the dimensionless equilibrium conditions can be written as

$$\tilde{P}_b' - \tilde{P}_{IOP} = \frac{2T(f)}{R(f)\Delta P} \quad \text{and} \tag{12}$$

$$f \geqslant \frac{1}{\tilde{U}_* + 1} \equiv f_*, \tag{13}$$

respectively. Note that the adhesion energy alone fixes possible values of the shape parameter f which determines the normalized blister cross-sectional profile. For $h(0) \leqslant R$, basic geometry gives the blister profile as a function of $f \geqslant 1/2$:

$$\frac{h(\tilde{r})}{R_\perp} = \sqrt{\frac{1}{4f(1-f)} - \tilde{r}^2} - \sqrt{\frac{1}{4f(1-f)} - 1}. \tag{14}$$

Figure 5 plots the normalized blister height $h(\tilde{r})/R_\perp$ as a function of the normalized radial coordinate $\tilde{r} = r/R_\perp$ for various values of the adhesion energy $\tilde{U}_*$.

In cases where the maximum height $h(0) > R$ ($f < 1/2$), similar equations for blisters with overhangs can be derived. The blister becomes more bulbous for larger adhesion energies $\tilde{U}_*$, with the transition from a blister with $h(0) < R$ to one with an overhang occurring when f falls below $1/2$. From equation (13), this occurs for $\tilde{U}_* > 1$, and is illustrated by the $\tilde{U}_* = 3$ example in figure 5. For the sake of simplicity, we have neglected the bending rigidity of the detached retinal layer which can be estimated by $\kappa_B \approx \frac{1}{12}Ed^3/(1-\nu^2) \approx Ed^3/9$, where $\nu \approx 1/2$ is Poisson's ratio of the fairly incompressible

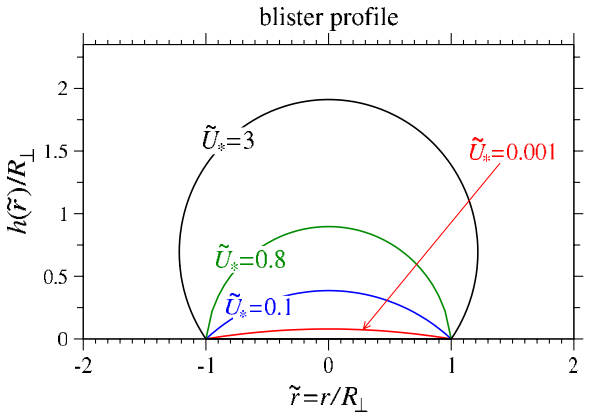

Figure 5. The blister profile plotted for various normalized adhesion energies $\tilde{U}_*$. Note that the blister shape depends only on the normalized adhesion energy $\tilde{U}_*$, while the radius $R_\perp$ is a function of all other parameters in the problem.

retinal tissue [20]. Incorporation of bending forces would smooth the kink of the retinal surface across the point of contact. The width of this transition region scales as $\sqrt{\kappa_B/T} \sim d/\sqrt{\tilde{U}_*}$ [21] which, using typical parameters from table A1 (appendix) yields $d/(R\sqrt{\tilde{U}_*}) \ll 1$ for small $\tilde{U}_*$ and fairly flat blisters. Therefore, the inclusion of retinal bending forces will not qualitatively affect the shape of the blister and we henceforth neglect it.

Equation (13) only provides a condition for the blister shape. To determine the blister size, we must now solve Laplace's pressure jump equation (equation (12)) while preserving the condition $f \geqslant (\tilde{U}_* + 1)^{-1}$ found above from balancing the tension with the retinal adhesion energy. Equation (12) imposes an additional constraint on the physical parameters $\tilde{J}_p$, $\tilde{L}_r$ and $\tilde{U}_*$, which can only be satisfied for certain blister radius $R_\perp$. We now specify two models for $P'_b - P_{IOP}$. We will first assume that a circular region of some radius $R_\perp$ has been previously mechanically detached and that within this footprint, the molecular bonds have been irreversibly broken, and the physiological state under the blister is uniform. A relationship for the pressure difference $P'_b - P_{IOP}$ can be found by imposing volume conservation under the blister $A_r L_r(P'_b - P_{IOP}) = A_d L_c(P_c - P'_b) - A_d J_p$. The dimensionless form of equation (12) becomes

$$\frac{(1-\tilde{J}_p)}{\tilde{L}_r + f} = \lambda_\perp \left(\frac{1}{f} - 1\right)^{3/2}, \quad \lambda_\perp \equiv \left(\frac{4Ed}{R_\perp \Delta P}\right). \tag{15}$$

Solving equation (15) with $f \geqslant f_*$ yields a finite blister footprint radius $R_\perp$ only if $(\tilde{L}_r + f)(1/f - 1)^{3/2} > (1-\tilde{J}_p)/\lambda_\perp$. This constraint defines a critical blister radius

$$R_\perp^{cr} = \left(\frac{4Ed}{\Delta P}\right) \frac{[\tilde{L}_r(\tilde{U}_* + 1) + 1]\tilde{U}_*^{3/2}}{(\tilde{U}_* + 1)(1 - \tilde{J}_p)}, \tag{16}$$

above which no stable solution to $R_\perp$ exists. Pre-formed blisters with $R_\perp \leqslant R_\perp^{cr}$ are stable while those with footprint radius $R_\perp > R_\perp^{cr}$ are unstable. To maintain the same stable blister pressure P'_b (so that net volume flow into the blister remains zero) as the footprint radius $R_\perp$ increases requires that the curvature of the detached retina remains constant. Therefore, stability requires that f decreases and the blister becomes more bulbous. Beyond a certain critical radius $R_\perp^{cr}$, the small-f, bulbous blister can no longer be supported by the force condition $f \geqslant 1/(\tilde{U}_* + 1)$, and the blister spontaneously grows without limit.

Note that for sufficiently large pump fluxes such that $1 - \tilde{J}_p < 0$, there is no formal solution to equation (12) since any blister will be sucked flat onto the RPE, and eventually possibly heal itself. These results highlight the importance of the retina–choroid binding energy $\tilde{U}_*$ and of properly functioning RPE pumps. Sufficiently large binding energies $\tilde{U}_*$ impart stability to large areas of detachment, while RPE pumping that is effective enough to render $1 - \tilde{J}_p < 0$ spontaneously reabsorbs blisters regardless of the value of $\tilde{U}_*$. Using the typical parameter values listed in the appendix, it is typical that under normal physiological conditions $\tilde{J}_p \gtrsim 1$. Finally, note that equations (15) and (16) also apply to RPE detachments (as depicted in figure 1(*b*)), where the RPE is lifted off Bruch's membrane overlying the choroid and fluid is actively pumped *into* the blister. An RPE detachment would thus be described by our existing model, but with $J_p \to -J_p$, and $\tilde{U}_*$ representing the RPE–Bruch membrane adhesion energy. The corresponding solution to $R_\perp$ (equation (16)) indicates that an RPE detachment can have a smaller critical radius $R_\perp^{cr}$ due to fluid pumping into the blister, or a larger $R_\perp^{cr}$ if the RPE–Bruch membrane adhesion is stronger than the retina–RPE adhesion.

For a second class of physiologically motivated detachment scenarios, we calculate the equilibrium size and shape of an exudative detachment that covers a circular choroidal/RPE lesion of known area A_ℓ (as shown in figure 4). In this case, the equilibrium blister size $R_\perp$ is not given by some past trauma, but is to be determined by stability conditions. Tissues within the lesion is in a different physiological state and have associated parameters L'_c, J'_p, and/or U'_* that can be different from L_c, J_p, and/or U_* of the non-lesioned tissue. For example, the RPE layer, Bruch's membrane, or choriocapillaris may be inflamed within the lesion, leading to a higher permeability, $L'_c > L_c$. The lesion may also represent tissue with lower RPE pump expression or function, rendering $J'_p < J_p$.

We now assume that retina over the lesion has lost adhesion ($\tilde{U}'_* = 0$). Upon balancing the total volume flux into the blister by summing the weighted volume flows associated with each tissue type (lesion or non-lesion):

$$\begin{aligned} A_r J_r &= A_\ell J'_c + (A_d - A_\ell)J_c - A_\ell J'_p - (A_d - A_\ell)J_p \\ &= A_r L_r(P'_b - P_{IOP}). \end{aligned} \tag{17}$$

Upon using the form $J'_c = L'_c(P_c - P'_b)$, defining the relative lesion area

$$g \equiv \frac{A_\ell}{A_r} \leqslant f \leqslant 1, \tag{18}$$

and solving equation (17) for the dimensionless transretinal pressure jump $\tilde{P}'_b - \tilde{P}_{IOP}$, we re-express equation (12) in a dimensionless form:

$$\frac{(f-g) + g\tilde{L}'_c - (f-g)\tilde{J}_p - g\tilde{J}'_p}{\tilde{L}_r + (f-g) + g\tilde{L}'_c} = \frac{2T(f)}{R\Delta P}. \tag{19}$$

Since the lesion radius $R_\ell = \sqrt{A_\ell/\pi}$ is constant, we express the radius of curvature as $R(f,g) \equiv R_\ell/\sqrt{4g(1-f)}$. Upon

using equation (9) for $T(f)$, equation (19) can be rewritten in the form of a cubic equation for the ratio $g \equiv A_\ell/A_r$:

$$\sqrt{f}\Lambda(f)\frac{(1-\tilde{L}'_c)}{(\tilde{L}_r+f)}g^{3/2}+[\tilde{L}'_c-1+\tilde{J}_p-\tilde{J}'_p]g - \sqrt{f}\Lambda(f)\sqrt{g}+f(1-\tilde{J}_p)=0, \quad (20)$$

where $\Lambda(f) \equiv \lambda_\ell(1/f-1)^{3/2}(\tilde{L}_r+f)$ and $\lambda_\ell \equiv \left(\frac{4Ed}{R_\ell \Delta P}\right)$ are convenient dimensionless combinations of parameters. By solving equation (20) for g as a function of f, λ_ℓ, $\tilde{L}'_c$, $\tilde{J}_p$ and $\tilde{J}'_p$, we can find the parameter range that supports steady-state blisters, and the precise shape and size of the detachment. In this scenario, we assume that the blister grows until the tension is exactly balanced (the equality in equation (7)) so that the operative value of the shape parameter is $f=(\tilde{U}_*+1)^{-1}\equiv f_*$, leading to the dimensionless control parameter

$$\Lambda(f_*)\equiv\Lambda_*=\lambda_\ell\tilde{U}_*^{3/2}\left(\tilde{L}_r+\frac{1}{\tilde{U}_*+1}\right). \quad (21)$$

Without loss of generality, further analytic progress can be made in a number of physiologically relevant subcases. First, assume the RPE cell layer becomes locally more permeable to fluid flow ($\tilde{L}'_c > 1$) and the adhesion outside the lesion is also weak. Solving equation (20) in the small Λ_* limit for the physical root g_*, we find a stable blister footprint radius

$$\tilde{R}_\perp \equiv \frac{R_\perp}{R_\ell}=\sqrt{\frac{f_*}{g_*}}\approx\sqrt{\frac{\tilde{L}'_c-1+\tilde{J}_p-\tilde{J}'_p}{\tilde{J}_p-1}} \quad (22)$$

only when $\tilde{J}_p > 1$. Figure 6(*a*) plots $\tilde{R}_\perp$ as a function of $\tilde{J}_p$ for various $\tilde{L}'_c-\tilde{J}'_p$. As expected, detached blisters increase in size as lesion conductivity increases, and diminish in size as RPE pumping $\tilde{J}_p$ increases.

A more complex situation arises if the choroidal permeability within the lesion is approximately that of healthy tissue ($L_c = L'_c$ and $\tilde{L}'_c = 1$) and the pump flux in the lesion tissue $\tilde{J}'_p \approx 0$. In this case, equation (20) reduces to $\tilde{J}_p g-\sqrt{f_*}\Lambda_*\sqrt{g}+f_*(1-\tilde{J}_p)=0$. Upon finding the physical root g_*, we construct a normalized blister footprint radius

$$\tilde{R}_\perp=\frac{2\tilde{J}_p}{\Lambda_*+\sqrt{\Lambda_*^2-4\tilde{J}_p(1-\tilde{J}_p)}} \quad (23)$$

which depends on only two dimensionless parameters, the dimensionless healthy-tissue RPE pump flux $\tilde{J}_p$, and the parameter combination Λ_*. A real, stable solution to equation (23) exists only if $\Lambda_*^2 \geqslant 4\tilde{J}_p(1-\tilde{J}_p)$. Once this condition is no longer satisfied, the blister radius $\tilde{R}_\perp \to \infty$. Furthermore, equation (23) is valid only when $\tilde{R}_\perp \geqslant 1$. When the parameters are such that the blister footprint shrinks to below that of the lesion, the problem becomes one of fixed blister radius R_ℓ and equation (16) applied, but with $R_\perp$ interpreted as R_ℓ.

For RPE pump fluxes $\tilde{J}_p > 1$, fluid in the subretinal space is sufficiently evacuated such that the blister radius $\tilde{R}_\perp$ is always finite. The retina is held down by the healthy-tissue RPE pumps and even when $\tilde{U}_*$ (and hence Λ_*) vanish, the blister radius $\tilde{R}_\perp \to \sqrt{\tilde{J}_p/(\tilde{J}_p-1)}$. However, when $\tilde{J}_p < 1$, stability of the blister relies on the chorioretinal adhesion energy. For sufficiently low $\tilde{U}_*$, the blister becomes unstable and grows without bound. For example, if $\tilde{U}_*$ is decreased to the point that $\Lambda_* = 2\sqrt{\tilde{J}_p(1-\tilde{J}_p)}$, $\tilde{R}_\perp \to \sqrt{\tilde{J}_p/(1-\tilde{J}_p)}$. If Λ_* is further decreased (for example, by decreasing λ_ℓ and/or $\tilde{U}_*$), the blister becomes unstable and $\tilde{R}_\perp \to \infty$.

For sufficiently large Λ_*, the retina is always stable. When $\Lambda_* > 1$, the physical solution g_* is such that $\tilde{R}_\perp = 1$ indicating that the blister radius has contracted to within the boundary of the lesion, and no retina above healthy choroid tissue is detached. The shape of a fully contracted blister in this regime is determined only by $f_* = (\tilde{U}_*+1)^{-1}$, where the value of $\tilde{U}_*$ is found from solving equation (21) when $\Lambda_* = 1$:

$$\tilde{U}_* = \begin{cases} (\lambda_\ell \tilde{L}_r)^{-2/3} & \lambda_\ell \tilde{L}_r \ll 1, \\ (\lambda_\ell(\tilde{L}_r+1))^{-2/3} & \lambda_\ell \tilde{L}_r \gg 1. \end{cases}$$

The first case arises when, for example, the retina is highly stretchable and/or impermeable. Here, $\tilde{U}_*$ is large, f_* is small and the blister is bulbous in shape. In the opposite limit of permeable and/or stiff retinas, $f_* \lesssim 1$, indicating that the blister is relatively flat.

When $\Lambda_* < 1$, and $\tilde{J}_p < 1/2\left[1+\sqrt{1-\Lambda_*^2}\right]$, the blister pressure $P'_b - P_{IOP}$ cannot be balanced by the retinal tension term and the blister is unstable to unbounded growth $\tilde{R}_\perp \to \infty$. Only when $\tilde{J}_p > 1/2\left[1+\sqrt{1-\Lambda_*^2}\right]$ is a finite blister footprint radius stable. Our results are summarized in figure 6(*b*), where values of $\tilde{R}_\perp$ are shown in the $\Lambda_* - \tilde{J}_p$ plane. For a more detailed plots representing equation (23), see the appendix.

5. Discussion and conclusions

We have developed a mathematical framework to describe exudative retinal detachments. Forces arising from hydraulic pressure differences, active and passive fluid flow and cellular adhesion are balanced to determine the stability conditions of a uniform retinal layer. We find that spontaneous retinal detachment occurs whenever equation (5) is satisfied. Using realistic parameter values, we find that spontaneous, uniform tissue separation can occur only if both the RPE pumps fail and the retina–RPE adhesion energy are globally reduced.

A more realistic scenario involves a localized exudative detachment, or blister, under which subretinal fluid has accumulated [15]. One of our main findings is that the *shape* of the blister depends only on the stretching elasticity of the detached retinal sheet and the adhesion energy per area between the retina and the RPE. To find the size, or footprint radius $R_\perp$, of the blister, the pressure difference across the detached retina must be balanced with the geometry-dependent tension of the retina. We consider two clinically relevant scenarios. The first assumes that a circular patch of retina has been detached from an unspecified external force (such as vitreous shear forces or transient normal tension forces through collagen fibers that may be attached to the retina). The physiological properties (adhesion strength, choroidal hydraulic conductivity and RPE pump flux) under the detached region may be different from those in the normal undetached region. In this scenario, we find a critical blister radius $R_\perp^{cr}$ above which the blister is unstable to further growth. Estimates for $R_\perp^{cr}$ range from millimeters to a centimeter, although the

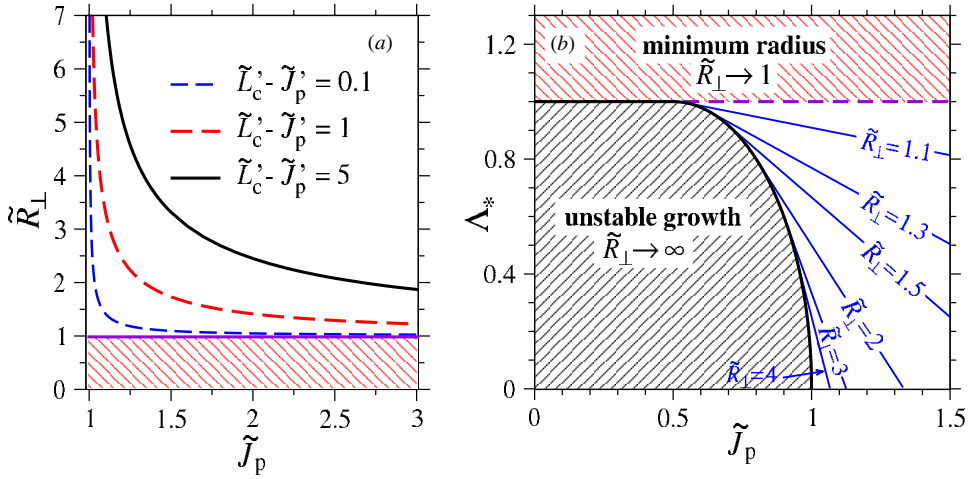

Figure 6. (*a*) Plot of $\tilde{R}_\perp$ (equation (22)) in the weak adhesion ($\tilde{U}_* \approx \tilde{U}_*' \approx 0$) and leaky lesion ($\tilde{L}_c' > 1$) limit. (*b*) Contour plot of $\tilde{R}_\perp$ (equation (23)) as functions of the RPE pump flux $\tilde{J}_p$ and the dimensionless combination Λ_*. Three qualitatively different regimes for $\tilde{R}_\perp$ are clearly indicated. For $\Lambda_* > 1$, the physical solution g_* is such that $\tilde{R}_\perp = 1$ indicating that the blister radius has contracted to the boundary of the lesion. For $\Lambda_* < 1$, and $\tilde{J}_p < 1/2\left[1 + \sqrt{1 - \Lambda_*^2}\right]$, the blister pressure $P_b' - P_{IOP}$ cannot be balanced by the retinal tension term and the blister is unstable to unbounded growth $\tilde{R}_\perp \to \infty$. Only when $\tilde{J}_p > 1/2\left[1 + \sqrt{1 - \Lambda_*^2}\right]$ is a finite blister footprint radius stable.

actual critical radius may be larger due to restoring forces from vitreous tamponading, which we neglect.

In the second scenario, we assume a localized circular lesion of radius R_ℓ, above which the retina is already detached from e.g. prior trauma. The physiological parameters in the lesion differ from the rest of the healthy tissue. Here, the blister footprint radius is determined by the physical solution to a cubic equation and other constraints. Two relevant subcases with simple analytic results arise. When the substrate tissue within the lesion is leaky and $\tilde{L}_c' > 1$ (for example, if the tight junctions of the RPE monolayer are locally disrupted), the blister radius in the weak adhesion limit ($\Lambda_* \approx 0$) is determined by equation (22) and is plotted in figure 6(*a*). In the case where the RPE pump flux is not affected by the inflamed tissue, the resulting quadratic equation can be solved to find the blister radius as a function of the dimensionless combination Λ_* (equation (21)) and $\tilde{J}_p = J_p/(L_c \Delta P)$. Here, blister sizes are delineated in ($\tilde{J}_p$, Λ_*) space in figure 6(*b*), while the more detailed dependences of $\tilde{R}_\perp = R_\perp/R_\ell$ on Λ_* and $\tilde{J}_p$ are illustrated in figure A3 in the appendix.

Our model for blister formation relates the physiological state of the retinal and choroidal tissue to physical parameters such as intraocular and vascular pressures, hydraulic conductivity, adhesion strength, retinal elasticity and RPE pump flux. Some of these parameters can be experimentally or clinically altered using e.g., anti-inflammatory drugs to decrease hydraulic conductivities, or intraocular pressure lowering drugs to decrease P_{IOP}. Retinal detachments under different physiological and structural conditions can also be compared using the mechanical principles quantified in our model. Our analyses can potentially guide the clinical prediction, prevention and repair of exudative retinal detachments.

Acknowledgments

TC is grateful to Dr Elena Bitrian of the Jules Stein Eye Institute for illuminating discussions and the Oppenheimer Foundation for a seed grant. Part of this project was conceived and developed in the Institute for Pure and Applied Mathematics, UCLA. The authors were also supported by the Army Research Office through grant 58386MA (TC), and National Science Foundation through grants DMS-1032131 (TC), DMS-1021818 (TC), DMS-1009105 (MS) and DMS-1016406 (MS).

Appendix

A.1. Relevant physiological parameters

The parameter values, including values for the elasticity of detached retina, are taken from different experiments performed on dog, pig, rabbit and human retina. While the parameter values in table A1 vary greatly, we nonetheless use them as rough guides to the magnitude of the forces detailed in our modeling. The variability in the parameters

Table A1. Table of measured parameter values. Note that 1 mm Hg is equivalent to 133 Pa = 133 N m^{-2}.

Physical parameter	Symbol	Typical values	Reference
Intraocular pressure	P_{IOP}	10–20 mm Hg	[6, 7]
Vascular pressure	P_c	15–25 mm Hg	[9, 23]
Blister pressure	P_b	$P_c > P_b > P_{IOP}$	[9, 15]
Retinal conductivity	L_r	10^{-7}, 10^{-10} m/(Pa s)	[24]
Choriodal conductivity	L_c	10^{-8}, 10^{-9} m/(Pa s)	[25]
RPE pump flux	J_p	$\sim 10^{-8}$ m s^{-1}	[7, 11]
Retina–RPE adhesion	U_*	~ 0.1 J m^{-2}	[14, 15, 22]
Retinal Young's modulus	E	10^3, 10^4, 10^5 Pa	[26–28]
Retinal thickness	d	$\sim$ 100–250 μm	[7]

arises from measurements across different animals, possibly different tissue layers, using different experimental techniques and sample preparation protocols.

For example, the retinal elasticity E appears to be highly sensitive on whether it was measured using mechanical stretching [27, 28], indentation force microscopy [29], with the force indentation results giving lower values of $E \sim 1$ kPa, more consistent with a neural tissue.

Similarly, the retina–RPE adhesion energy U_* is typically obtained by measuring the force required to separate the retina from the RPE. However, the force required to separate the layers will depend on the RPE pump activity, which would need to be carefully subtracted from the applied force in order to obtain the intrinsic, pump-free adhesion energy. The range of values observed is ~ 0.01–0.1 J m^{-2} which is on the order of that of an air–water interface.

A.2. Angle-dependent detachment condition

The precise balancing of tension and adhesion forces at the edge of a blister will depend on the microscopic details of how macromolecular bonds are oriented and adhere the retinal cells to the stiff choroid. For example, if the bonds are free to 'swivel', then the cells detach when the magnitude T of the tension exceeds that of the binding energy per area U_*. This case is described by equation (7) and the analyses subsequent to it. However, if the bond-rupturing coordinate is, say, normal to the retina then the binding energy per area is balanced by only the normal component $T\sin\theta$ of the retina tension. Since the bonds (or the cells themselves) holding the retinal cells can be ruptured by forces along different bond-rupture 'coordinates', we interpolate between the total force and normal force rupturing modes by defining the parameter α through the force balance equation

$$T\sqrt{\alpha\cos^2\theta+\sin^2\theta} \approx U_* - z_*(P_b - P_{IOP}) \approx U_*, \tag{A.1}$$

where the angle θ is the contact angle the retinal makes at the perimeter of detachment and can be related to the blister radius through $R_\perp/R = \sin\theta$. Upon expressing the tension T and θ in terms of the shape factor f, we find

$$\frac{1-f}{f}\sqrt{\alpha+4(1-\alpha)f(1-f)} \leqslant \tilde{U}_*. \tag{A.2}$$

As the case with equation (13), the shape parameter $f \geqslant f(\tilde{U}_*;\alpha)$ depends only $\tilde{U}_*$ and α. If $\alpha = 1$, the magnitude of the tension T contributes to cell detachment and we recover equation (13). However, for $\alpha = 0$, only the normal component of T acts to detach the retinal cells. In this case, we find

$$f(\tilde{U}_*;\alpha=0) \equiv \frac{A_d}{A_r} = 1 - \frac{\tilde{U}_*^{4/3}}{6}\left(\sqrt{1+\frac{\tilde{U}_*^2}{27}}-1\right)^{-1/3} + \frac{\tilde{U}_*^{2/3}}{2}\left(\sqrt{1+\frac{\tilde{U}_*^2}{27}}-1\right)^{2/3}. \tag{A.3}$$

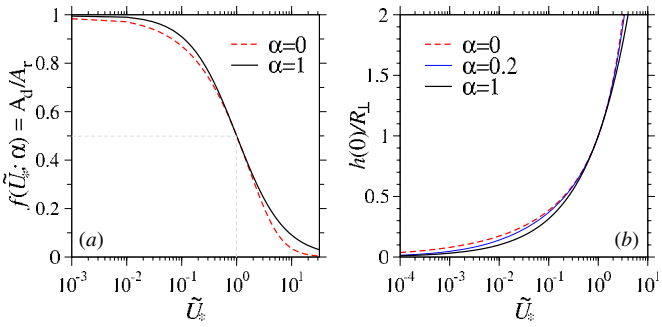

Figure A1. (*a*) The blister shape parameter $f(\tilde{U}_*;\alpha) \equiv A_d/A_r$ as a function of the normalized retinal adhesion energy per area $\tilde{U}_* = U_*/(Ed)$ (solid curve). Shape parameters for both normal force ($\alpha = 0$) and total force ($\alpha = 1$) rupturing mechanisms are shown. (*b*) The maximum height $h(0)/R_\perp$ plotted as a function of $\tilde{U}_*$ for various α. The dependence on α is modest.

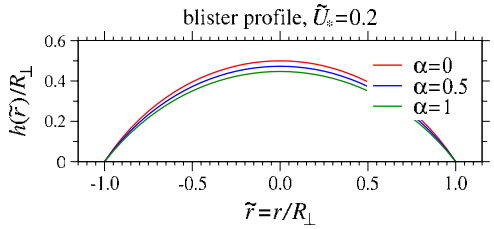

Figure A2. Change in the blister profile for varying α and fixed $\tilde{U}_* = 0.2$. When only the normal component of tension induces detachment ($\alpha = 0$), larger retinal stretching is required at the stable contact perimeter (red curve).

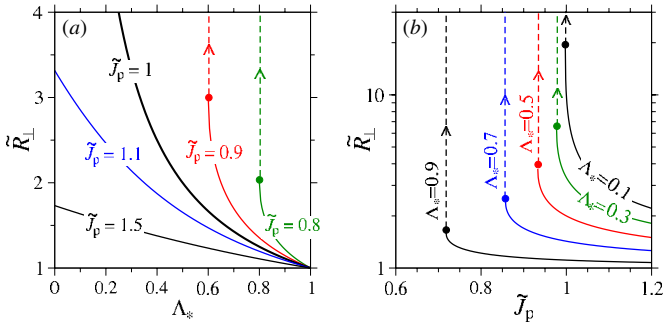

Figure A3. (*a*) The normalized blister radius $\tilde{R}_\perp$ as a function of Λ_* at various dimensionless rescaled RPE pump fluxes $\tilde{J}_p = 0.8, 0.9, 1, 1.1, 1.5$. (*b*) The normalized blister radius $\tilde{R}_\perp$ as a function of the normalized RPE pump flux $\tilde{J}_p$ for various values of $\Lambda_* = 0.1, 0.3, 0.5, 0.7, 0.9$.

For irreversible delamination, these solutions $f(\tilde{U}_*;\alpha)$ provide a lower bound for the appropriate shape factor f and are plotted in figure A1(*a*). The dashed curves in figure A1 shows $f(\tilde{U}_*;\alpha=0)$. Intermediate values of α yield ratios A_d/A_r that interpolate between the plotted curves. Figure A1(*b*) shows the relative height of the blister for various α. Note that the effect of the rupture mode α on the blister shape is minimal except at large $\tilde{U}_* \gtrsim 3$, where the relative difference becomes appreciable.

To illustrate the effects of the retinal detachment mode on the allowed shapes, in figure A2 we plot $h(\tilde{r})/R_\perp$ at a fixed adhesion energy $\tilde{U}_*$ for $\alpha = 0, 0.5, 1$. Although for $\alpha = 0$, the

complicated expression for $f(\tilde{U}_*; \alpha = 0$ does yield the simple analytic expressions for $\alpha = 1$ derived in the main body of this paper, figures A1 and A2 show that the different modes of detachment do not qualitatively alter our overall results except in the extreme case where $\tilde{U}_* \gtrsim 3$ and blisters have overhangs.

A.3. Analysis of $\tilde{R}_\perp(\Lambda_*, \tilde{J}_\mathrm{p})$

For completeness, we plot slices of the solution $\tilde{R}_\perp(\Lambda_*, \tilde{J}_\mathrm{p})$ in figure A3. Figure A3(*a*) plots the expected normalized blister footprint radius $\tilde{R}_\perp$ (equation (23)) as a function of the dimensionless combination Λ_* and various values of the normalized, rescaled, RPE pump flux $\tilde{J}_\mathrm{p}$. $\tilde{R}_\perp$ increases with decreasing Λ_*, and in particular, for $\tilde{J}_\mathrm{p} < 1$, there is an abrupt transition to instability and $\tilde{R}_\perp \to \infty$, at the points indicated by the solid dots. This plot is qualitatively similar to a plot where Λ_* is replaced by $\lambda_\ell \tilde{U}_*^{3/2}(\tilde{L}_\mathrm{r} + 1)$ (for $\tilde{U}_* \ll 1$) or $\lambda_\ell \tilde{U}_*^{3/2}\tilde{L}_\mathrm{r}$ (for $\tilde{U}_* \gg 1$).

Figure A3(*b*) shows $\tilde{R}_\perp$ as a function of $\tilde{J}_\mathrm{p}$ for fixed Λ_*. For each fixed Λ_*, as $\tilde{J}_\mathrm{p}$ is decreased, $\tilde{R}_\perp$ increases. Less effective RPE pumps lead to larger blisters. Below a critical $\tilde{J}_\mathrm{p}$, the radius $\tilde{R}_\perp$ growth without bound at a maximum permissible radius (dots).

References

[1] Yanoff M and Duker J S 1999 *Ophthalmology* (London: Mosby International)

[2] Williamson T H 2008 *Vitreoretinal Surgery* (Berlin: Springer)

[3] Foster W J, Dowla N, Joshi S Y and Nikolaou M 2010 The fluid mechanics of scleral buckling surgery for the repair of retinal detachment *Graefes Arch. Clin. Exp. Ophthalmol.* **248** 31–6

[4] Stopa M, Lincoff A and Lincoff H 2007 Analysis of forces acting upon submacular hemorrhage in pneumatic displacement *Retina* **27** 370–4

[5] Marmor M F 1988 New hypotheses on the pathogenesis and treatment of serous retinal detachment *Graefes Arch. Clin. Exp. Ophthalmol.* **226** 548–52

[6] Brubaker R F 1982 The flow of aqueous humor in the human eye *Trans. Am. Ophthalmol. Soc.* **80** 391–474

[7] Ethier C R, Johnson M and Ruberti J 2004 Ocular biomechanics and biotransport *Ann. Rev. Biomed. Eng.* **6** 249–73

[8] Goel M, Picciani R G, Lee R K and Bhattacharya S K 2010 Aqueous humor dynamics: a review *Open Ophthalmol. J.* **4** 52–9

[9] Maepea O 1992 Pressures in the anterior ciliary arteries, choroidal veins and choriocapillaris *Exp. Eye Res.* **54** 731–6

[10] Starita C *et al* 1996 Hydrodynamics of ageing Bruch's membrane: implications for macular disease *Exp. Eye Res.* **62** 565–72

[11] Tsuboi S 1987 Measurement of the volume flow and hydraulic conductivity across the isolated dog retinal pigment epithelium *Invest Ophthalmol. Vis. Sci.* **28** 1776–82

[12] Fatt I 1975 Flow and diffusion in the vitreous body of the eye *Bull. Math. Biol.* **37** 85–90

[13] Fatt I and Shantinath K 1971 Flow conductivity of retina and its role in retinal adhesion *Exp. Eye Res.* **12** 218–26

[14] Zauberman H and Berman E R 1969 Measurement of adhesive forces between the sensory retina and the pigment epithelium *Exp. Eye Res.* **8** 276–83

[15] Kain H L 1984 A new model for examining chorioretinal adhesion experimentally *Arch. Ophthalmol.* **102** 608–11

[16] Wang C Y 1986 A critical review of the heavy elastica *Int. J. Mech. Sci.* **28** 549–59

[17] Vella D, Boudaoud A and Adda-Bedia M 2009 Statics and inertial dynamics of a ruck in a rug *Phys. Rev. Lett.* **103** 174301

[18] Kolinski J M, Aussillous P and Mahadevan L 2009 Shape and motion of a ruck in a rug *Phys. Rev. Lett.* **103** 174302

[19] Wagner T J W and Vella D 2011 Floating carpets and the delamination of elastic sheets *Phys. Rev. lett.* **107** 044301

[20] Landau L D and Lifshitz E M 1959 *Theory of Elasticity* (Oxford: Pergamon)

[21] Powers T R, Huber G and Goldstein R E 2002 Fluid-membrane tethers: minimal surfaces and elastic boundary layers *Phys. Rev.* E **65** 041901

[22] Maurice D M, Salmon J and Zauberman H 1971 Subretinal pressure and retinal adhesion *Exp. Eye Res.* **12** 212–7

[23] Maurice D M 1987 Flow of water between aqueous and vitreous compartments in the rabbit eye *Am. J. Physiol. Renal. Physiol.* **252** F104–8

[24] Antcliff R J, Hussain A A and Marshall J 2001 Hydraulic conductivity of fixed retinal tissue after sequential excimer laser ablation *Arch. Ophthalmol.* **119** 539–44

[25] Moore D J, Hussain A A and Marshall J 1995 Age-related variation in the hydraulic conductivity of Bruch's membrane *Invest Ophthalmol. Vis. Sci.* **36** 1290–7

[26] Jones I L, Warner M and Stevens J D 1992 Mathematical modelling of the elastic properties of retina: a determination of Young's modulus *Eye* **6** 556–9

[27] Wollensak G and Eberhard S 2004 Biomechanical characteristics of retina *Retina* **24** 967–70

[28] Reichenbach A, Eberhardt W, Scheibe R, Deich C, Seifert B, Reichelt W, Dahnert K and Rodenbeck M 1991 Development of the rabbit retina: IV. Tissue tensility and elasticity in dependence on topographic specializations *Exp. Eye Res.* **53** 241–51

[29] Franze K, Francke M, Guenter K, Christ A F, Koerber N, Reichenbach A and Guck J 2011 Spatial mapping of the mechanical properties of the living retina using scanning force microscopy *Soft Matter* **7** 3147–54